Biophysical Journal, Volume *117*

Supplemental Information

Critical Structural Defects Explain Filamin A Mutations Causing Mitral Valve Dysplasia

Tatu J.K. Haataja, Romain Capoulade, Simon Lecointe, Maarit Hellman, Jean Merot, Perttu Permi, and Ulla Pentikäinen

Table S1. Primary SAXS data processing of the FLNA4-6 and the mutated fragments related to Figure 2 in this study. The SAXS data were deposited to Small Angle Scattering Biological Data Bank (SASBDB) for public access. Both of the mutated fragments display concentration dependency that can be seen from increasing R_g, D_{max} and $I(0)$ values. This is likely a consequence from increased protein aggregation.

	FLNA4-6			FLNA4-6 V711D			FLNA4-6 H743P		
	1 mg/ml	**2 mg/ml**	**4 mg/ml**	**1 mg/ml**	**2 mg/ml**	**4 mg/ml**	**1 mg/ml**	**2 mg/ml**	**4 mg/ml**
Guinier analysis									
$I(0)$ (arbitary units)	23.0 ± 0.05	23.7 ± 0.03	24.0 ± 0.02	24.1 ± 0.07	26.9 ± 0.05	30.8 ± 0.06	23.4 ± 0.07	28.5 ± 0.06	32.1 ± 0.05
R_g (nm)[a]	2.7 ± 0.01	2.7 ± 0.01	2.7 ± 0.01	3.7 ± 0.02	4.0 ± 0.18	4.1 ± 0.02	3.8 ± 0.02	4.0 ± 0.02	4.3 ± 0.02
s_{min} (nm^{-1})	0.42	0.42	0.40	0.36	0.22	0.53	0.37	0.32	0.36
sR_g max (nm^{-1})	1.27	1.22	1.22	1.20	1.04	1.03	1.19	1.09	1.02
Coefficient of correlation, R^2	0.998	0.998	0.999	0.997	0.997	0.999	0.997	0.997	0.998
MW from $I(0)$ (kDa) (ratio to predicted)[b]	22.4 (0.71)	23.1 (0.73)	23.4 (0.74)	24.5 (0.78)	26.2 (0.84)	30.0 (0.96)	22.1 (0.71)	27.8 (0.89)	31.3 (1.00)
P(r) analysis									
$I(0)$ (arbitary units)	23.3 ± 0.04	24.0 ± 0.02	24.1 ± 0.02	24.0 ± 0.06	26.7 ± 0.05	30.8 ± 0.03	23.5 ± 0.06	28.6 ± 0.05	32.2 ± 0.03
R_g (nm)	2.8 ± 0.08	2.8 ± 0.05	2.8 ± 0.01	3.8 ± 0.01	4.0 ± 0.01	4.2 ± 0.09	3.9 ± 0.02	4.2 ± 0.01	4.4 ± 0.01
D_{max} (nm)[c]	9.7	9.7	9.7	12.5	14.8	15.0	14.0	15.3	16.0
s range (nm^{-1})	0.105 - 3.327	0.081 - 3.327	0.128 - 3.327	0.119 - 3.327	0.128 - 2.856	0.128 - 3.798	0.105 - 3.325	0.105 - 3.325	0.081 - 3.327
X^2 (total estimate from GNOM)	0.95 (0.84)	0.91 (0.83)	0.93 (0.83)	0.96 (0.69)	0.92 (0.73)	0.99 (0.60)	0.94 (0.75)	0.92 (0.58)	0.99 (0.74)
Predicted MW (kDa)[d]		31.5			31.5			31.5	
MW from $I(0)$ (kDa) (ratio to predicted)[b]	22.7 (0.72)	23.4 (0.74)	23.5 (0.75)	23.4 (0.74)	26.1 (0.83)	30.1 (0.96)	22.9 (0.73)	27.9 (0.89)	31.4 (1.00)
Porod volume, V_P (nm^3)[e]	40.6	41.5	41.2	49.6	57.1	64.9	57.8	61.1	66.7
MW from V_P (kDa) (ratio to predicted)[f]	24.5 (0.78)	25.0 (0.79)	24.8 (0.79)	29.9 (0.95)	34.4 (1.09)	39.1 (1.24)	34.8 (1.10)	36.8 (1.17)	40.2 (1.28)
SASBDB codes		SASDFD3[g]			SASDFF3	SASDFE3		SASDFH3	SASDFG3

[a] Estimated from Guinier analysis in PRIMUS (1)

[b] Calculated by comparing to standard BSA (c = 4.38 mg/ml), MW = 66.4 kDa, $I(0)$ 68.06 (arbitary units) using the formula $MW_X/I(0)_X = MW_{BSA}/I(0)_{BSA}$

[c] Calculated using DATGNOM (2)

[d] Estimated from the amino acids sequences using ExPasy ProtParam tool, https://web.expasy.org/protparam/

[e] Calculated using DATPOROD (3)

[f] MW = V/1.66 (4)

[g] Merged scattering data of 2 mg/ml and 4 mg/ml deposited

Table S2. Shape-model fitting results related to Figure 3 in this study. The obtained *ab initio* and rigid body models of FLNA4-6 fit well against the experimental scattering data. The DAMMIF and SASREF models were deposited to SASBDB along with the experimental scattering data under SASBDB ID SASDFD3.

	FLNA4-6[a]	FLNA4-6 models
DAMMIF[b] *via ATSAS* online (default parameters, 20 calculations)		
s range for fitting (nm^{-1})	0.1565 - 2.8492	
Symmetry, anisotropy assumptions	P1, prolate	
NSD (standard deviation), number of clusters	0.957 (0.039), 6	
X^2 range	0.850 - 0.857	
Constant subtracted	0.0558	
Resolution (Å, from SASRES)[c]	30 ± 2	
MW estimate as 0.5 x volume of models (kDa) (ratio to expected)	28.0 (0.89)	
SASREF[d] *via ATSAS* online (default parameters)		
s range for fitting (nm^{-1})		0.0741 - 3.129
Symmetry		P1
No. of curves (No. of experimental points)		1 (650)
No. of subunits		2
Subunit 1 (range)		4M9P (574-766)
Subunit 2 (range)		FLNa6 model (767-869)
Final X^2		0.92
CORAL[e] *via ATSAS online* (default parameters)		
s range for fitting (nm^{-1})		0.0741 - 2.658
Symmetry		P1
No. of curves (No. of experimental points)		1 (550)
No. of subunits		2
Subunit 1 (range); fixed		4M9P (574-766)
Subunit 2 (range)		FLNa6 model (767-869)
Linker region		762 - 771
Number of calculated models		50
Final X^2 (range)		0.92 - 1.09
CRYSOL[f] *via ATSAS* online (default parameters)		
Origin of the rigid body model		SASREF
Constant subtraction		allowed
X^2, *CORMAP P-value*		0.992, 0.000
Predicted R_g (Å)		28.64
Vol (Å), Ra (Å), Dro ($e\ Å^{-3}$)		35784, 1.44, 0.048

[a] Merged experimental scattering data of 2 mg/ml and 4 mg/ml used

[b] https://www.embl-hamburg.de/biosaxs/atsas-online/dammif.php (5)

[c] https://www.embl-hamburg.de/biosaxs/atsas-online/dammif.php (6)

[d] https://www.embl-hamburg.de/biosaxs/atsas-online/sasref.php (7)

[e] https://www.embl-hamburg.de/biosaxs/atsas-online/coral.php (8)

[f] https://www.embl-hamburg.de/biosaxs/atsas-online/crysol.php (9)

Table S3. Quantitative EOM analyses of the SAXS data of FLNA4-6 and theV711D and H743P mutants related to Figure 2 in this study. The EOM analyses of the FLNA3-5 fragment have been added for direct comparison to the FLNA4-6 fragments. All the final ensembles give comparable R_g and D_{max} values with the primary data processing of the studied proteins. FLNA4-6 displays more inherent flexibility based on the R_{flex} (random)/R_{sigma} values than FLNA3-5, suggesting that FLNA6 domain is more flexible than FLNA3. The experimental data from both of the mutants give good fits when FLNA6 model is utilized in the calculations, suggesting that the structure of the FLNA6 domain is not significantly affected by the point mutations in the neighboring FLNA5 domain. The FLNA3-5 and FLNA4-6 data are also in good agreement with the obtained *ab initio* models of the proteins, since FLNA4-6 (SASBDB ID SASDFD3) displays significantly elongated shape when compared to the compact FLNA3-5 (SASBDB ID SASDEQ7). The qualitative EOM analyses of the FLNA3-5 fragment have been previously reported by Haataja et al. (10).

	FLNA4-6[a]	**FLNA4-6 V711D[b]**	**FLNA4-6 H743P[b]**	**FLNA3-5[ac]**
EOM[d] (Default parameters, 10 000 models in the initial ensemble)				
s range for fitting (nm^{-1})	0.0741 - 1.623	0.0741 - 1.585	0.0506 - 1.585	0.0506 - 1.599
Type of models generated	native-like	random coil	random coil	native-like
Domain 1 (range)	4M9P (574-766)	-	-	4M9P (478-573)
Domain 2 (range)	FLNA6 model (767-869)	FLNA6 model (767-869)	FLNA6 model (767-869)	4M9P (574-668)
Domain 3 (range)	-	-	-	4M9P (669-766)
X^2, *CORMAP P-value*	0.878, 0.146	0.842, 0.142	0.959, 0.019	0.774, 0.038
Constant subtracted	0.023	0.127	0.033	0.146
No. of representative structures	4	14	17	2
R_{flex} (random) / R_{sigma}	81.9% (87.5%) / 1.3	87.8 % (84.9%) / 1.2	87.3 % (84.4%) / 1.2	58.2% (89.0%) / 0.5
Final ensemble R_g/D_{max} (nm)	2.8/9.2	4.4/14.0	4.5/14.3	2.2/7.0

[a] Merged experimental scattering data of 2 mg/ml and 4 mg/ml used

[b] Experimental scattering data from 4 mg/ml used

[c] Graphical EOM data published previously by Haataja *et al.* (10)

[d] https://www.embl-hamburg.de/biosaxs/atsas-online/eom.php (11, 12)

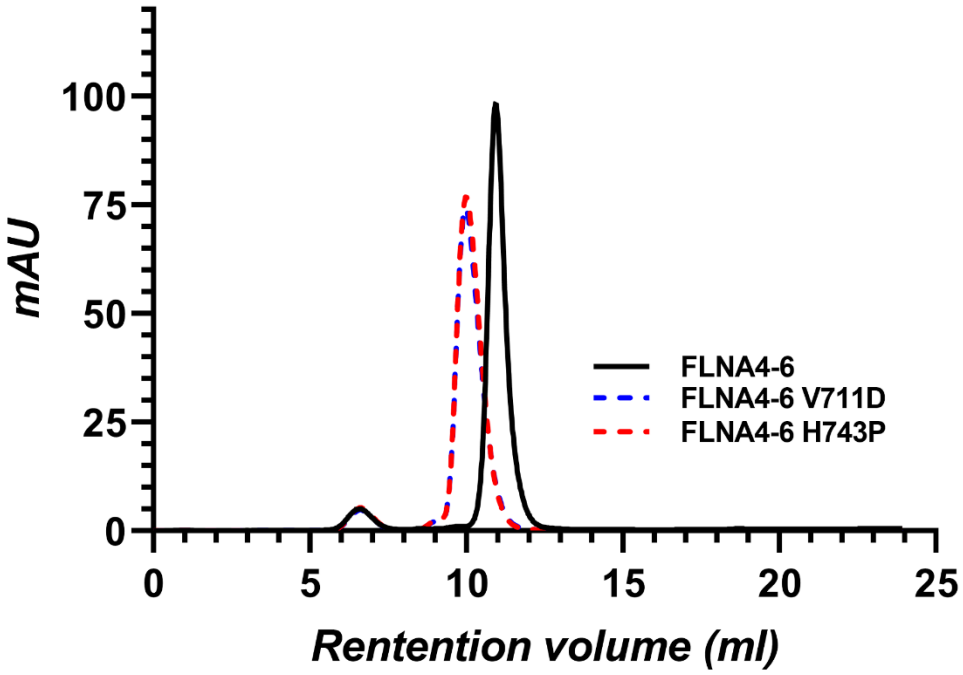

Figure S1. Analytical gel filtration profiles of FLNA4-6 and the mutated fragments, V711D and H743P, related to Figure 2 in this study. 500 µg of purified protein was injected into Superdex 75 HR 10/30 column (GE Healthcare) equilibrated in 20 mM Tris; pH 8.0, 100 mM NaCl, 1 mM DTT. The protein was eluted at 500 µl/min for 1 column volume at room temperature.

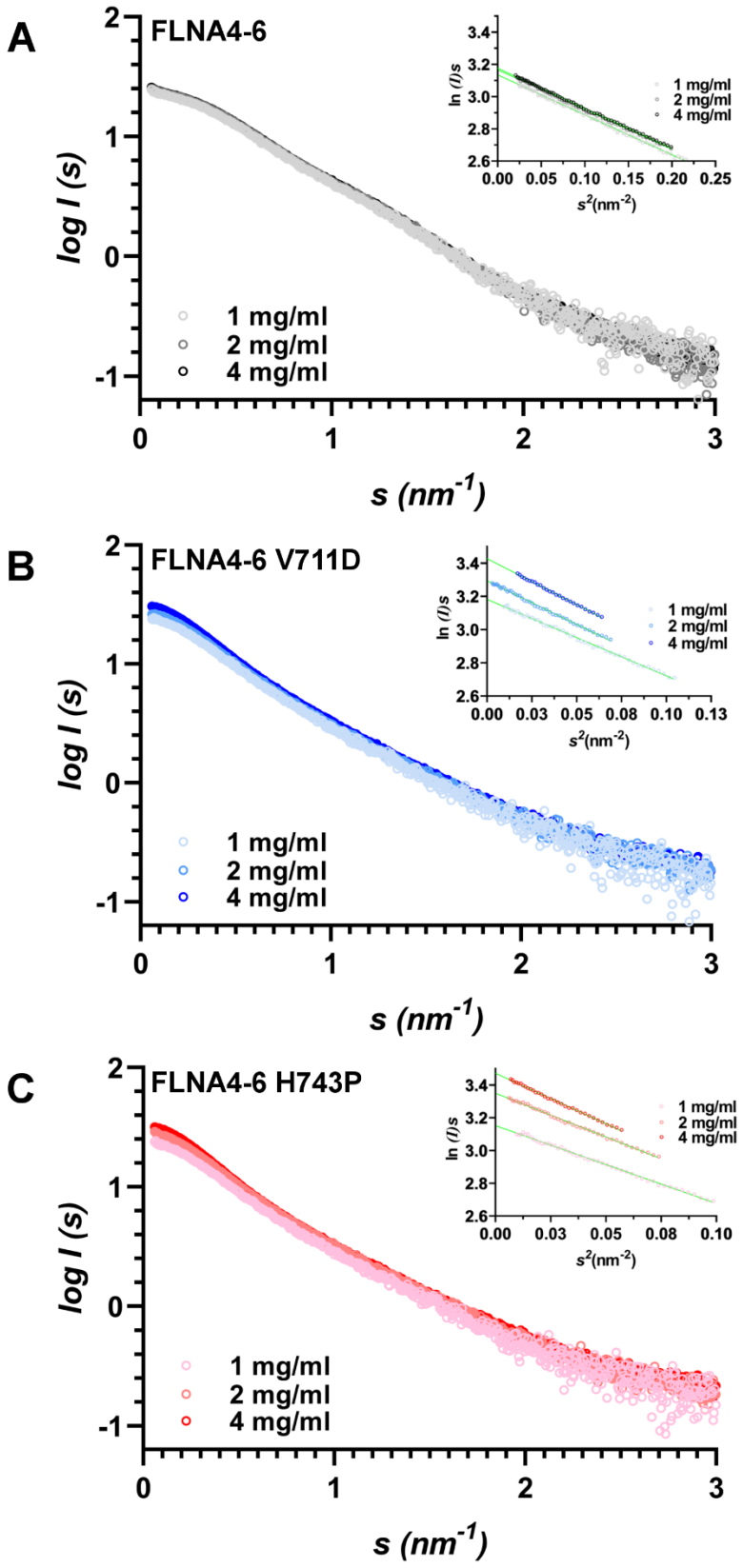

Figure S2. Primary small angle X-ray scattering (SAXS) analysis of FLNA4-6 and the mutated fragments related to Figure 2 in this study. The solution scattering profiles with the insets showing the Guinier fits of (*A*) FLNA4-6, (*B*) FLNA4-6 V711D and (*C*) FLNA4-6 H743P at 1, 2 and 4 mg/ml concentrations. Both of the mutated fragments display concentration dependency in the Guinier fits that is likely a consequence from increased protein aggregation.

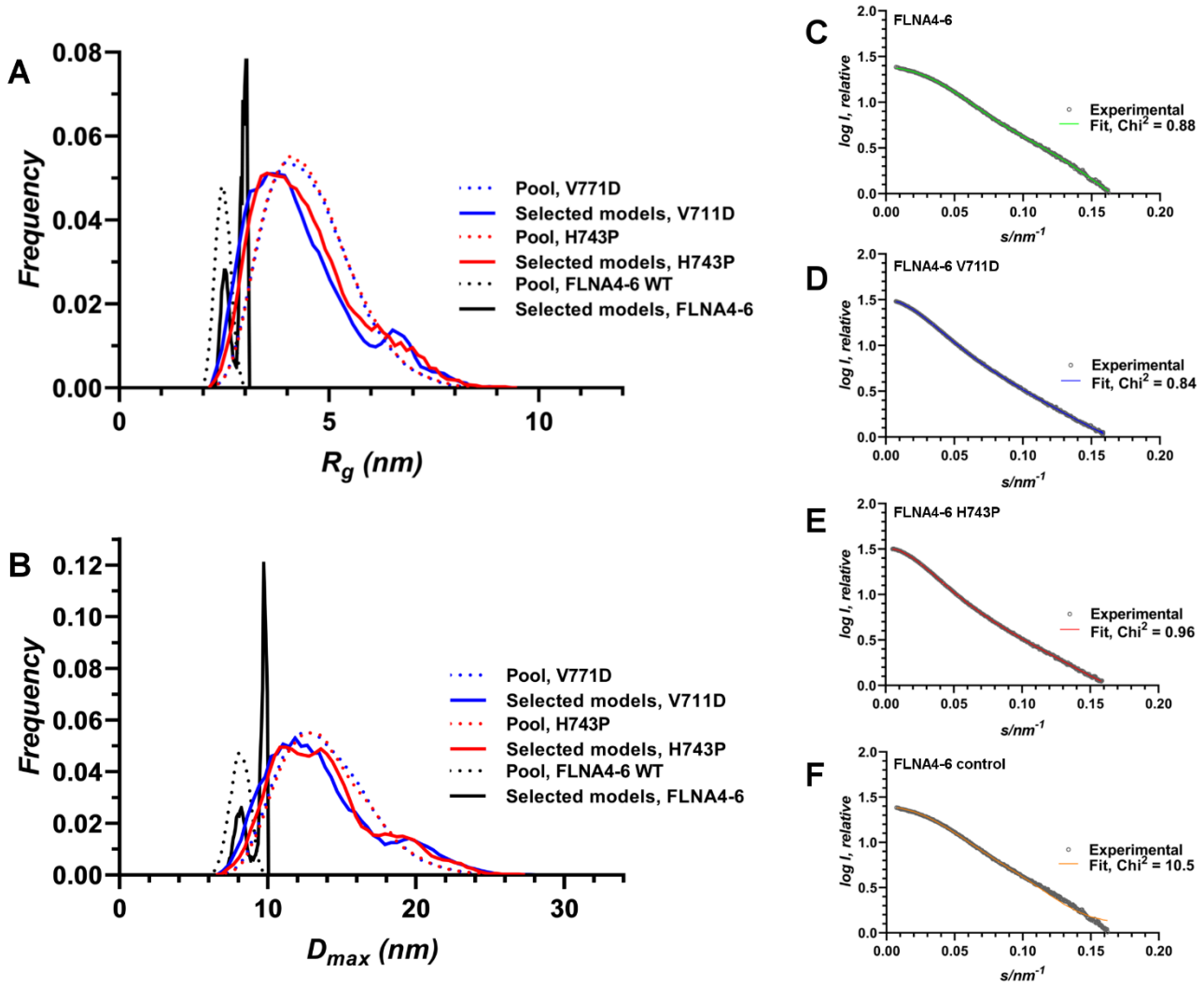

Figure S3. Comparing the inherent protein flexibility of FLNA4-6 and the mutated fragments by ensemble optimization method (EOM) related to Figure 2 in this study. The EOM analyses of the SAXS data of FLNA4-6 and the mutants, V711D and H743P, demonstrate that both of the mutations significantly increase the inherent flexibility of the FLNA4-6 fragment. In the case of FLNA4-6 fragment, the pool represents the structures calculated based on the sequence and crystal structures of FLNA4-5 domain pair and the homology model of FLNA6, while the mutant data was analyzed using the sequence information for FLNA4-5 domain pair and the homology model of FLNA6. In addition, a control analysis was performed for the FLNA4-6 data using the EOM setup identical to the mutants. The selected models in *A* and *B* represent structures within the pool that fit to the experimental scattering curve. (*A*) Radius of gyration (R_g) distribution and (*B*) maximum dimension of the particle (D_{max}) distribution histograms of the selected conformers versus the pool obtained from EOM calculations of the FLNA4-6 (black), FLNA4-6 V711D (blue) and FLNA4-6 H743P (red). Typical fits obtained from the selected ensemble of structures to experimental scattering of (*C*) FLNA4-6, (*D*) FLNA4-6 V711D, (*E*) FLNA4-6 H743P and (*F*) FLNA4-6 control. The major broadening of the R_g and D_{max} distributions of the selected conformers is an indication of increase of the inherent flexibility of the mutated FLNA4-6 fragments. As expected, the FLNA4-6 control in which FLNA4-5 domain pair is random coil and only the FLNA6 domain is structured does not fit to the FLNA4-6 experimental scattering data (*F*).

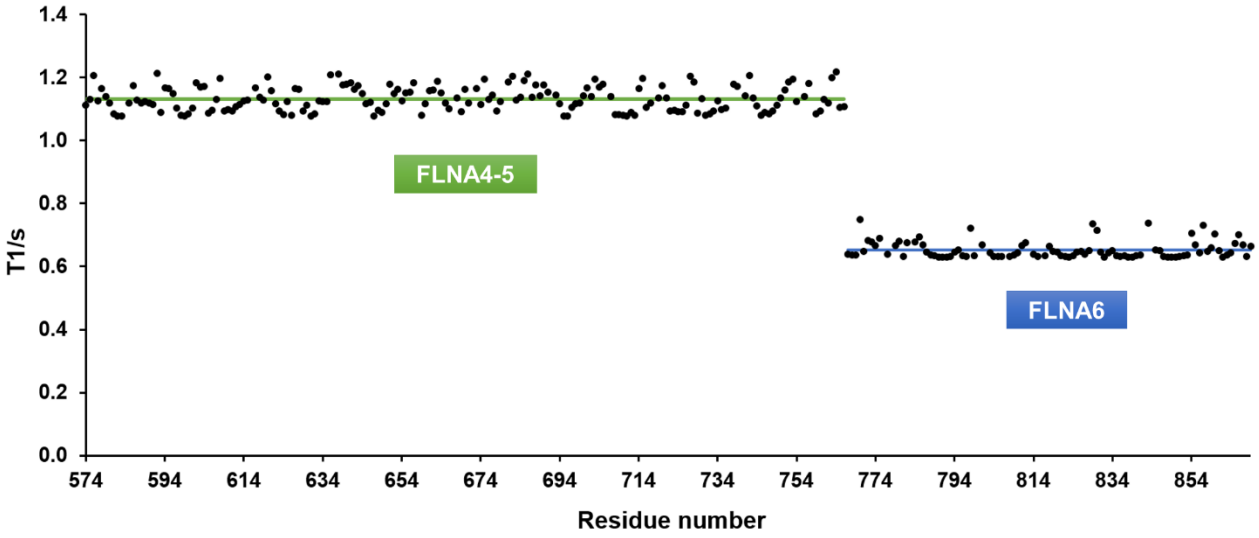

Figure S4. FLNA6 is not part of the compact rod1 fragment related to Figure 3 in this study. The plot of ^{15}N T_1 simulated relaxation times for FLNA4-5 and FLNA6 versus the FLNA4-6 amino acid sequence using HYDRONMR software (13). The results clearly indicate that FLNA4-5 moves together but independently from FLNA6. The theoretically calculated values are well in agreement with experimental values shown in Figure 3 *A*. Horizontal lines indicate the average value calculated for FLNA4-5 and FLNA6.

SUPPLEMENTARY REFENCES

(1) Konarev, P. V., V.V. Volkov, …, D. I. Svergun 2003. PRIMUS: a Windows PC-based system for small-angle scattering data analysis. *J. Appl. Cryst.* 36: 1277–1282.

(2) Petoukhov, M.V., P. V. Konarev, …, D. I. Svergun 2007. ATSAS 2.1-Towards automated and web-supported small-angle scattering data analysis, *J. Appl. Cryst.* 40: 223–228.

(3) Franke, D., M. V. Petoukhov, …, D. I. Svergun 2017. ATSAS 2.8: a comprehensive data analysis suite for small-angle scattering from macromolecular solutions, *J. Appl. Cryst.* 50: 1212–1225.

(4) Rambo, R.P. and J.A. Tainer 2011. Characterizing flexible and intrinsically unstructured biological macromolecules by SAS using the Porod-Debye law, *Biopolymers.* 95: 559-571.

(5) Franke, D. and D. I. Svergun 2009. DAMMIF, a program for rapid ab-initio shape determination in small-angle scattering, *J. Appl. Cryst.* 42: 342-346.

(6) Tuukkanen, A.T., G. J. Kleywegt and D. I. Svergun 2016. Resolution of ab initio shapes determined from small-angle scattering, *IUCrJ.* 3: 440-447.

(7) Petoukhov, M.V. and D. I. Svergun 2005. Global rigid body modelling of macromolecular complexes against small-angle scattering data, *Biophys J.* 89: 1237-1250.

(8) Petoukhov, M.V., D. Franke, …, D.I. Svergun 2012. New developments in the ATSAS program package for small-angle scattering data analysis, *J. Appl. Cryst.* 45: 342-350.

(9) Svergun, D.I., C. Barberato and M. H. J. 1995. CRYSOL – a Program to Evaluate X-ray Solution Scattering of Biological Macromolecules from Atomic Coordinates, *J. Appl. Cryst.* 28: 768-773.

(10) Haataja, T.J.K., R. C. Bernardi, …, U. Pentikäinen 2019. Non-syndromic Mitral Valve Dysplasia Mutation Changes the Force Resilience and Interaction of Human Filamin A, *Structure.* 27: 102–112.e4.

(11) Tria, G., H. D. T. Mertens, …, D. I. Svergun 2015. Advanced ensemble modelling of flexible macromolecules using X-ray solution scattering. *IUCrJ.* 2: 207-217.

(12) Bernado, P., E. Mylonas, …, D. I. Svergun 2007. Structural Characterization of Flexible Proteins Using Small-Angle X-ray Scattering. *J Am Chem Soc.* 129: 5656-5664.

(13) Schuler, B. 2018. Perspective: Chain dynamics of unfolded and intrinsically disordered proteins from nanosecond fluorescence correlation spectroscopy combined with single-molecule FRET, *J. Chem. Phys.* 149: 1–10.